Generalized reconstruction model of SiC(001)-($n\times2$) surfaces and Si ad-dimer strings

Peter Krüger and Johannes Pollmann
Institut für Festkörpertheorie, Universität Münster, D-48149 Münster, Germany
(Received 1 September 2005; revised manuscript received 30 November 2005; published 24 January 2006)

We report *ab initio* calculations on the atomic and electronic structure of the 7×2 and 8×2 surfaces of cubic SiC(001) carried out within local density approximation of the density functional theory. Supercells, nonlocal norm-conserving pseudopotentials and Gaussian orbital basis sets are used to describe the surface systems. Our results for the surface structure are in good accord with a lot of experimental data. These investigations complement our previous *ab initio* studies on $c(4\times2)$, 3×2 and 5×2 reconstructions of the SiC(001) surface. On the basis of all our results, we suggest a general two adlayer asymmetric dimer model (TAADM) for $n\times2$ reconstructions of SiC(001). The model is based on two structural building blocks. The first contains an asymmetric dimer in one partial adlayer while the second contains an asymmetric dimer configuration of six Si adatoms in two partial adlayers. These are characteristic for the $c(4\times2)$ and 3×2 reconstructions, respectively. Employing the model for higher n values allows us to suggest optimal structures for a large host of $n\times2$ reconstructions. Comparing the formation energies of the $c(4\times2)$ and all $n\times2$ structures considered, we find in agreement with experiment that the 3×2 and $c(4\times2)$ reconstructions are most favorable for silicon-rich and silicon-poor growth conditions, respectively. The formation energies of all other reconstructions fall in between these two limits. In particular, the general TAADM allows us to rationalize the occurrence of periodic and nonperiodic Si ad-dimer-string arrangements at Si-terminated 3C-SiC(001) surfaces in very good accord with experimental data.

DOI: 10.1103/PhysRevB.73.035327 PACS number(s): 68.35.Bs, 73.20.At, 68.35.Md

I. INTRODUCTION

Silicon carbide (SiC) is a wide-band-gap semiconductor of large fundamental and technological interest because of its unique chemical, mechanical, electronic, and optical properties making it very attractive for the fabrication of high-power and high-frequency electronic devices, as well as of light emitters which can operate under harsh conditions.[1,2] SiC is very different from usual group-IV semiconductors, in particular, because of the largely different covalent radii of Si and C and a respectively strong ionicity. As a consequence, SiC exists in many polytypes. Of these polytypes, cubic and hexagonal SiC and their surfaces are the most relevant for applications. They have been investigated in great detail, therefore (cf. Refs. 1–9). A rich variety of reconstructions of the 3C-SiC(001) surface has been found depending sensitively on the stoichiometry of the surface. For the C-terminated surface, the $c(2\times2)$ bridging dimer reconstruction is favored.[10–17] For silicon-rich Si-terminated surfaces, $n\times2$ reconstructions with odd $n=3,5,7,\ldots$ have been observed,[18–21] while for silicon-poor Si-terminated surfaces $c(4\times2)$ or 2×1 reconstructions have been identified.[12,18,22–28]

More recently, the formation of Si lines at SiC(001) surfaces has been discovered.[29–33] Such one-dimensional subnanometer structures are expected to be of considerable interest for exploring novel nanoelectronic devices.[7,8] Using scanning tunneling microscopy (STM), Soukiassian and co-workers[29] observed the formation of straight, very long, and highly stable Si atomic lines self-organizing on the 3C-SiC(001) surface. Consisting of Si dimers, they were found to form at the phase transition from the silicon-rich 3×2 to the silicon-poor $c(4\times2)$ reconstruction by annealing a Si-saturated 3×2 surface at different temperatures for different times. The number and spacing of the Si lines, crucially depending on surface preparation conditions, is mediated by annealing time and temperature, resulting in unprecedented arrangements ranging from a very dense superlattice of parallel atomic lines to single isolated lines on top of the $c(4\times2)$ surface.[29–32] Subnanometer Si structures at SiC(001) have been detected, as well, by Kitamura *et al.*[33] who observed one-dimensional ad-dimer strings on $n\times2$ surfaces with n as large as 15. The latter authors went the opposite way to thermal annealing of a saturated 3×2 surface irradiating Si atoms by molecular beam epitaxy onto the silicon-poor $c(4\times2)$ surface and investigated the phase transition from the silicon-poor $c(4\times2)$ to the saturated 3×2 surface using STM. During the phase transition, a 15×2 structure, mixed 3×2 and 5×2 structures and a defective 3×2 structure have been seen. In the STM images of these structures periodic arrays of Si nanostrings in 3×2, 5×2, and 15×2 configurations are clearly visible.[33] Soukiassian's group has also observed Si dimer lines with long-range order occurring between the 3×2 and 5×2 surface orderings in an even 8×2 reconstruction of the SiC(001) surface.[30,31] This observation of an 8×2 reconstruction was largely unexpected in view of the fact that the Si-terminated SiC(001) surface had been thought until then to show only $n\times2$ reconstructions with n being odd (cf. Ref. 19). The very uncommon 8×2 reconstruction was interpreted as resulting from alternating 3×2 and 5×2 unit cells. These specific findings raise the point, whether $n\times2$ reconstructions of SiC(001) with even n are possible, in general, and if so, which kinds of Si nanolines are to be expected at such surfaces. This issue is of particular interest, in addition, since Hara *et al.*[19] have suggested a unified additional dimer-row model for SiC(001)

which predicts that even number $n\times2$ phases are unfavorable in terms of structural stability. The above experimental findings pose several basic questions: (a) How do SiC(001)-($n\times2$) surfaces reconstruct? (b) Why does SiC(001) show an 8×2 reconstruction in spite of the fact that neither 4×2 nor 6×2 reconstructions have been reported, to date?[5,8,19] (c) Why do Si nanostrings occur at various SiC(001) surfaces? (d) What is their microscopic nature and how are they bonded to the underlying surface? From a technological point of view, a detailed knowledge of $n\times2$ reconstructions and an understanding of the physical origin of ad-dimer-string formation at SiC(001) surfaces is an important issue for the feasible and improved device performance of such nanowire structures.

So far, no *ab initio* calculations of atomic and electronic properties of Si-terminated SiC(001)-($n\times2$) surfaces with $n>5$ have been reported. First-principles studies have been restricted to the 3×2 and 5×2 reconstructions, to date.[34–36] For higher $n\times2$ reconstructions, only empirical tight-binding calculations have been carried out by Shevlin *et al.*[36] These authors have used their first-principles results for the 3×2 reconstruction in a fitting procedure to obtain the tight-binding parameters needed for their empirical calculations on $n\times2$ surfaces. This mixed approach suffers from less controllable approximations[36] and does not treat different $n\times2$ reconstructions, which differ by relatively small formation energies only, on equal footing.

In this paper, we first address the 7×2 and 8×2 reconstructions of the Si-terminated SiC(001) surface by *ab initio* calculations in order to contribute to a detailed understanding of their structural and electronic properties. We discuss these reconstructions in light of our previous results on the $c(4\times2)$, 3×2, and 5×2 surfaces.[25,26,34,35] Analyzing our reconstruction models and formation energies of the latter surfaces, we observe that the 5×2 reconstruction consists of two simple structural building blocks characteristic for the $c(4\times2)$ and 3×2 surface reconstructions which we label *A*-type and *B*-type building blocks in the following. We find the 7×2 and 8×2 reconstructions to consist, as well, of particular configurations of these two building blocks, only. Encouraged by these observations, we then use these two building blocks to extrapolate our results to higher n values and to set up a general two adlayer asymmetric dimer model for higher $n\times2$ reconstructions. First, the model indicates in agreement with experiment[5,8,19] that neither a primitive 4×2 nor a 6×2 reconstruction should occur. Second, it predicts that higher $n\times2$ reconstructions with even $n\geqslant8$ are possible, as opposed to the earlier notion that only odd n reconstructions would occur.[19] Third, it suggests that the SiC(001)-(8×2) surface, on which Si ad-dimer lines have been observed,[30,31] consists of one *A*-type and two *B*-type units per 8×2 unit cell. Fourth, it explains the observed occurrence of periodic one-dimensional Si nanostrings on SiC(001)-($n\times2$) surfaces with $n=3$, 5, and 15, as observed by Kitamura *et al.*[33] Finally, the model indicates that a large variety of nonperiodic arrangements of Si nanostrings can occur on the SiC(001) surface depending sensitively on surface preparation conditions.

The paper is organized as follows. In Sec. II, we briefly outline the calculational method. In Sec. III, we present and discuss our results on structural and electronic properties of the 7×2 and 8×2 reconstructions in comparison with the previously investigated lower-index surfaces and with experiment. Section IV is devoted to the setup and a discussion of our general TAADM for SiC(001)-($n\times2$) surfaces. In Sec. V, we address the formation of nonperiodic arrangements of Si ad-dimer strings at SiC(001) surfaces. A short summary concludes the paper in Sec. VI.

II. CALCULATIONAL METHOD

The theoretical approach using supercells, Gaussian orbital basis sets and norm-conserving pseudopotentials in separable form has been described in more detail in Ref. 34. *Ab initio* pseudopotential calculations are carried out within local density approximation[37] of density functional theory (DFT-LDA). Nonlocal, norm-conserving pseudopotentials in separable form, as suggested by Kleinman and Bylander,[38] and the exchange-correlation functional of Ceperley and Alder,[39] as parametrized by Perdew and Zunger,[40] are employed in our calculations. For the carbon atom, a very smooth pseudopotential is used to reduce the numerical effort.[41] In each supercell, there is a slab of six atomic layers for SiC (three Si and three C layers) and one layer of hydrogen atoms terminating the broken bonds at the C bottom layer atoms to avoid artificial electronic gap states. In addition, two partial Si adlayers contain an appropriate number of Si adatoms. The slab in each supercell is separated by nine vacuum layers from its neighbors to avoid interactions across the vacuum. Thus, we describe the 7×2 or 8×2 surfaces with supercells containing 136 or 158 atoms, respectively. The wave functions are expanded in terms of linear combinations of Gaussian orbitals with s,p,d, and s^* symmetry. In our basis set, we use 30 Gaussian orbitals per surface-layer Si atom and per Si adatom. Moreover, we use 20 orbitals per atom for all other Si and C atoms in the supercell and 10 orbitals per saturating H atom. The decay constants for Si atoms in the slab are 0.2 and 0.6, while decay constants of 0.18, 0.5, and 1.0 have been used for Si atoms at the surface. For the C atoms, we use 0.35 and 1.7 and for the H atoms we use 0.35. All constants are given in atomic units. For each wave vector, e.g., the Hamiltonian matrix for the 8×2 surface is thus 3300×3300 in size. Integrals over the surface Brillouin zone (SBZ) are performed using the Monkhorst-Pack special **k**-point approach.[42] In the actual calculations, eight $\mathbf{k}_\parallel$-points in the SBZ turn out to be sufficient to obtain converged results. This is due to the fact that the fairly extended unit cells in real space lead to respectively small surface Brillouin zones in reciprocal space. To determine the optimal geometric structure, the atoms in the first three substrate-surface layers and in two partial Si adlayers are relaxed to eliminate the forces. The structure optimization is stopped when all forces in the system are smaller than 10^{-3} Ry/a.u. The modified Broyden scheme[43,44] is used in this optimization.

For a meaningful comparison of energy-optimized structures of surfaces with different adatom coverages, we calculate their grand canonical potential Ω. The *formation energy* of a particular surface is given by the difference of the grand

canonical potential of the respective reconstructed Si adatom structure and the corresponding clean ideal Si-terminated surface as[45,46]

$$E_f := \Delta\Omega = E - E_0 - \delta n \mu_{Si}, \quad (1)$$

where E and E_0 are the total energies of the reconstructed and the clean ideal surface, respectively, δn is the number of Si adatoms per unit cell for a specific reconstruction, and μ_{Si} is the Si chemical potential in the gas phase. It has an upper limit of $\mu_{Si(bulk)}$ and a lower limit of $\mu_{Si(bulk)} - \Delta H_f$ defining silicon-rich and silicon-poor preparation conditions, respectively. The heat of formation ΔH_f of cubic bulk SiC is 0.72 eV (cf. Ref. 34).

III. *AB INITIO* RESULTS

For convenience, we first summarize in Sec. III A, the basic structural properties of the $c(4\times2)$, 3×2, and 5×2 reconstructions. They serve as a reference for the discussion of our new *ab initio* results on the 7×2 and 8×2 reconstructions in Secs. III B and III C and as a basis for the setup of our general two adlayer asymmetric dimer model of all considered $n\times2$ reconstructions in Sec. IV.

A. Lower-index surfaces

Top views of the $c(4\times2)$ missing row asymmetric dimer (MRAD) model, as well as the 3×2 and 5×2 two adlayer asymmetric dimer (TAAD) models, as resulting from our previous DFT-LDA calculations,[25,26,34,35] are shown in Fig. 1. They are compared in detail in Ref. 9 with the pertinent literature and are found to be in good agreement with a host of experimental data and with other *ab initio* calculations where available.[47]

The $c(4\times2)$ MRAD model (top panel of Fig. 1) is characterized by half a monolayer of Si adatoms adsorbed on the complete terminating Si sublayer of the Si-terminated SiC(001) surface forming rows of buckled Si ad-dimers in the $\times2$ direction with every second row missing.[25,26] The Si sublayer is thus covered by 1/2 of a Si monolayer in this reconstruction. The asymmetric dimers are all tilted in the same direction. To minimize the total energy, they arrange in the staggered $c(4\times2)$ pattern, as shown in the top panel of Fig. 1. Per $c(4\times2)$ unit cell, there is one ad-dimer saturating the four dangling bonds on the Si sublayer giving rise to two dangling bonds, only. The building block of the $c(4\times2)$ reconstruction, which we label A, is indicated by the red square in the top panel of Fig. 1. It has a buckled Si ad-dimer (D_A) in its top layer. Note that the entire building block A is a box with the height of the supercell and the quadratic cross section defined by the red square in the top panel of Fig. 1. It is important to note that the respective sections of all lower lying layers in the box below the red square belong to the building block, as well. The A-block coordinates of the atoms in the adlayer and on the first three substrate layers determined by total energy minimization are given in the Appendix. Since the A blocks arrange at the $c(4\times2)$ surface in a staggered pattern, they do not coincide with the unit cell although they have the same volume.

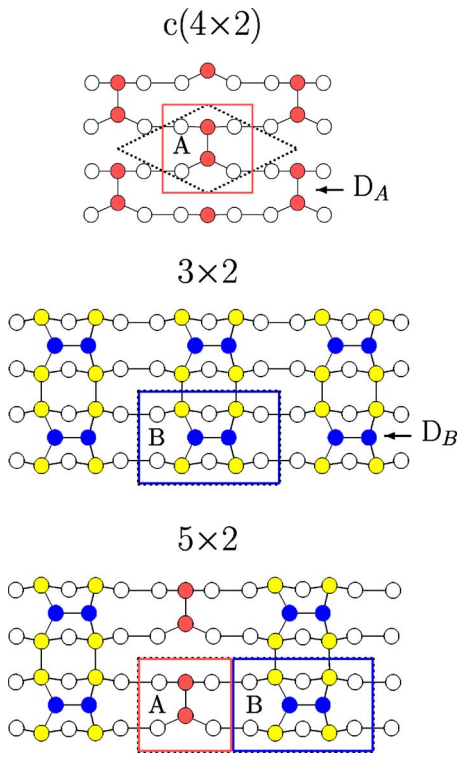

FIG. 1. (Color online) Top views of the optimized surface structure of the $c(4\times2)$ MRAD, as well as the 3×2 and 5×2 TAAD reconstructions of SiC(001). The atoms of the Si sublayer are shown by open circles. The building blocks A and B are indicated by red (gray) squares and blue (black) rectangles, respectively. For their definition, see text. The atoms of the D_A and D_B dimers are shown by red (gray) circles and blue (black) dots, respectively. The four Si atoms on the bottom adlayer of the 3×2 surface are shown by yellow (light gray) circles. The corresponding color code is used for the 5×2 surface. The unit cells are indicated by black dotted lines.

The 3×2 TAAD model (second panel of Fig. 1) has two partial Si adlayers above the terminating Si sublayer.[34] There are two Si adatoms per unit cell in the top adlayer forming buckled ad-dimers (D_B) in the $3\times$ direction and four Si adatoms in the bottom adlayer forming weak Si dimers in the $\times2$ direction. The latter adatoms saturate all dangling bonds on the Si sublayer. Thus, this reconstruction is also characterized by two dangling bonds per unit cell, only. The building block of the 3×2 reconstruction, which we label B, is indicated by the blue rectangle in the second panel of Fig. 1. In this case, the entire building block (B) is a box with the height of the supercell and the rectangular cross section defined by the blue rectangle in the middle panel of Fig. 1 having six Si adatoms in its two adlayers. The Si sublayer is thus covered by 1/3 and 2/3 of a Si monolayer from top to bottom. The B-block coordinates of the atoms in the two adlayers and on the first three substrate layers determined by total energy minimization are given in the Appendix, as well.

The 5×2 TAAD model (bottom panel of Fig. 1) contains one Si ad-dimer in the lower adlayer as in building block A and six Si adatoms on two adlayers as in building block B.[35] In the top adlayer there is only the D_B ad-dimer of the B-type building block while in the bottom adlayer there are the

lower four Si atoms of the B-type block and the D_A ad-dimer of the A-type building block. The bottom adlayer saturates all dangling bonds on the Si sublayer. Note that the D_A and D_B dimers are orthogonal to one another. The Si sublayer is now covered by 1/5 and 3/5 of a Si monolayer from top to bottom. The reconstruction is thus characterized by four dangling bonds per 5×2 unit cell. The 5×2 reconstruction can be viewed as a superposition of an A-type and a B-type building block. The bond lengths and bond angles of the dimers at the 5×2 surface deviate by less than 1% from the respective values in the A building block of the $c(4\times2)$ and the B building block of the 3×2 surface, respectively.[52] On the basis of these results, we expect that the 7×2 and 8×2 reconstructions are also characterized by appropriate superpositions of A-type and B-type building blocks.

In each of the above reconstructions, the Si sublayer bonds are fully saturated reducing the number of dangling bonds to a minimum. This is not the case for the $c(4\times2)$ alternatively up and down dimer (AUDD) model[12,47] or the 3×2 and 5×2 single dimer row model (SDRM), alternate dimer row model (ADRM), and double dimer row model (DDRM) suggested previously.[18,19,53,54] Our $c(4\times2)$, 3×2, and 5×2 models in Fig. 1 have by far the lowest formation energies, therefore, as compared to all other models suggested in the literature for the respective surfaces. For the 5×2 reconstruction, e.g., the SDRM and ADRM give rise to ten and the DDRM to eight dangling bonds per surface unit cell, respectively, while our TAADM features only four dangling bonds.

B. The SiC(001)-(7×2) surface

We now turn to the 7×2 surface. In order to contribute to a deeper understanding of its reconstruction, we have investigated a number of possible surface configurations by calculating their atomic structure and formation energy within density functional theory. In principle, many different reconstructions of a unit cell as large as that of the 7×2 surface are conceivable. We expect, however, that reconstructions with a minimum of surface dangling bonds are most likely. Previously, Hara *et al.*[19] have suggested also for the 7×2 surface a DDRM very similar in nature to their 5×2 DDRM. Like the latter, also the former has a very large number of dangling bonds, namely 12 per 7×2 unit cell. We expect this to be energetically very unfavorable. At the beginning of our calculations, we have distributed Si adatoms near positions in the 7×2 surface unit cell similar to their positions in one 3×2 and two $c(4\times2)$ unit cells to allow for a minimization of the number of surface dangling bonds. Starting the DFT-LDA total-energy minimization with such atom distributions, we end up with the optimized surface configuration shown in Fig. 2 by a top and a side view. Also for the 7×2 reconstruction, we find the TAADM to be a locally stable energy-minimum configuration. There are again two partial adlayers above the Si sublayer now with 1/7 and 4/7 of a Si monolayer from top to bottom. The atomic positions in the 7×2 unit cell turn out to be very similar to the respective positions in the A and B building blocks of the $c(4\times2)$ and 3×2 surface, respectively. There are only marginal deviations in

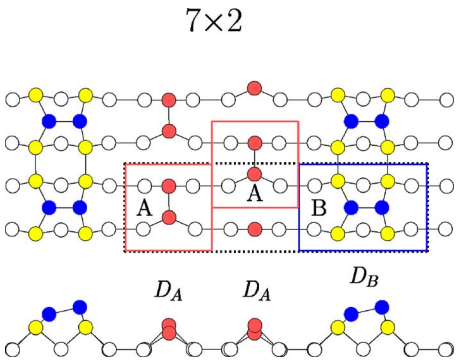

FIG. 2. (Color online) Top and side view of the optimal 7×2 TAAD model. A and B refer to the building blocks of the reconstruction, as discussed in Sec. III A. For details, see caption of Fig. 1.

atomic distances of less than 1%. Thus, the 7×2 reconstruction turns out to consist of one B-type and two A-type building blocks per 7×2 unit cell. The latter are arranged in the staggered pattern. The number of surface dangling bonds is 6, only, as opposed to the 12 dangling bonds[19] in the 7×2 DDRM. Therefore, our 7×2 TAADM should be energetically much more favorable. We have repeated the structure optimization for various initial positions of the Si adatoms in the general configuration of Fig. 2. In all cases, we end up with the same structure shown quantitatively in the figure.

The side view of the 7×2 surface (bottom panel of Fig. 2) clearly reveals that the D_B dimer occurs significantly higher above the surface than the two D_A dimers. While the latter reside at the same height, the D_B dimer occurs 1.295 Å above them. Therefore, the D_B dimers in the B-type building blocks are preferentially observable in filled-state STM images where they appear as a 7×2 periodic arrangement of Si ad-dimer lines along the $\times2$ direction interspaced by two channels of lower lying D_A dimer lines (see top panel of Fig. 2). Respective 7×2 ad-dimer line arrangements have been observed in experiment.[29,32] The authors estimated the ad-dimer lines to be located ≈2 Å above the missing dimer lines having the same structure as the Si dimer rows at the 3×2 surface. This is precisely what we find for our 7×2 *AAB* reconstruction. We note in passing that the height difference between the D_B and D_A dimers at the 5×2 surface results as 1.300 Å from our calculations.

Considering the top view of the 7×2 reconstruction in Fig. 2, it becomes obvious that there are probably other locally stable reconstruction configurations since there are several ways to arrange the two A-type building blocks in the 7×2 unit cell. We have scrutinized these additional possibilities and have considered a large number of Si adatom starting distributions of three different kinds. For each of these considered arrangements of A-type blocks, we arrive at one of the three locally stable energy-minimum configurations shown by top views in Figs. 3(b)–3(d). For convenience, we have included the top view from Fig. 2 in Fig. 3(a), as well. The common feature of these four configurations is that they are all TAAD reconstructions with only six surface dangling bonds consisting of one B-type and two A-type building blocks per unit cell differing only in finer details.

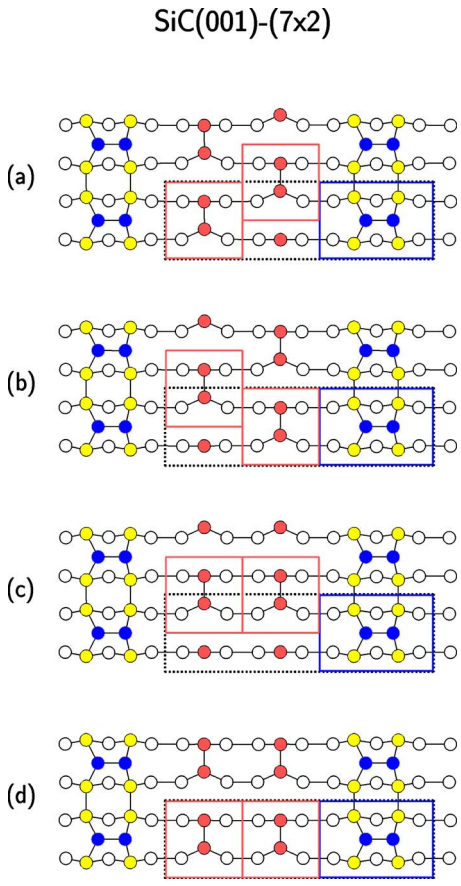

FIG. 3. (Color online) Top views of four investigated 7×2 TAAD reconstructions. The energy minimum structure (a) is in best general accord with experiment. The energy differences of the other structures relative to the one in (a) are +0.002 eV (b), +0.057 eV (c), and +0.064 eV (d). For details, see caption of Fig. 1.

Generally speaking, the two A units can be arranged in staggered ad-dimer configurations [Figs. 3(a) and 3(b)] or in ad-dimer row configurations [Figs. 3(c) and 3(d)]. The staggered ad-dimer configurations are characteristic for the $c(4\times2)$ surface (see top panel of Fig. 1). Configuration (b) differs from (a) only by an opposite staggering of the two A blocks along the $\times2$ direction, or (which is the same) by a shift of the two staggered A blocks by half a surface lattice constant along the $\times2$ direction. Nevertheless, the physical character of the two staggered A configurations in the 7×2 unit cell is largely equivalent. In fact, configuration (b) is only 0.002 eV higher in energy than (a). This marginal energy difference indicates that there is almost no interaction between adlayer atoms belonging to the two different A-type and the B-type building blocks, while all lower lying layers of the building blocks obviously have practically the same bond connectivity and bond interactions as in the SiC sublattice of the $c(4\times2)$ and 3×2 surfaces.

If we consider Si adatom distributions in two A-type units arranged in rows along the $7\times$ direction as in configurations (c) and (d), the resulting optimized structures are very close in energy but they are 0.057 eV and 0.064 eV higher in energy, respectively, than configuration (a). Configuration (d) differs from (c) only by a shift of the two A-type units by half a surface lattice constant along the $\times2$ direction. In both latter cases, the row arrangement of the two A-type units corresponds to that of the 2×2 MRAD reconstruction.[55] It turns out that the energy increase of configurations (c) and (d) with respect to (a) is basically the same as that of the 2×2 MRAD model with respect to the $c(4\times2)$ MRAD model. We find the 2×2 MRAD model to be 0.055 eV higher in energy than the $c(4\times2)$ MRAD model. This is due to the fact that the occupied dangling-bond states at neighboring dimer up atoms of the 2×2 reconstruction experience a noticeable Coulomb repulsion. On the contrary, in the staggered $c(4\times2)$ MRAD configuration, every up atom of one dimer has only down atoms of neighboring dimers as its neighbors (see top panel of Fig. 1) whose dangling-bond orbitals are empty so that the above mentioned repulsion is strongly reduced. Thus, there is also, in this case, a very small residual interaction energy of 0.007 eV at most between adlayer atoms belonging to different A-type and B-type building blocks of the 7×2 reconstruction models (c) and (d).

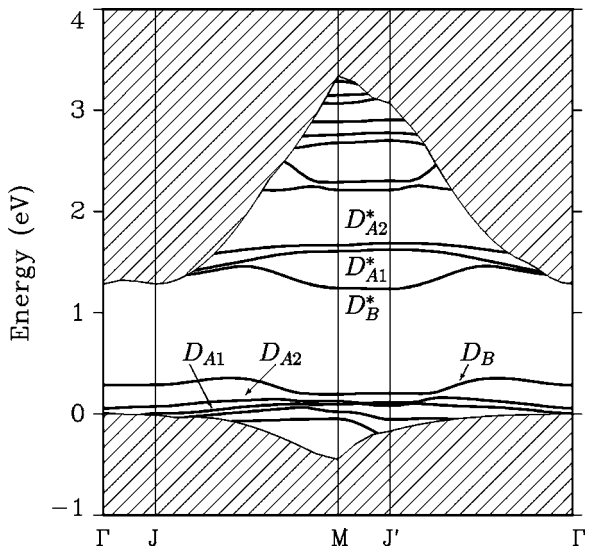

FIG. 4. Surface electronic structure of the TAADM of SiC(001)-(7×2) according to Fig. 2. The shaded areas show the projected bulk band structure.

Summarizing, we find in accord with experiment, a stable total energy minimum structure of the 7×2 surface [Figs. 2 and 3(a)] consisting of one B-type and two A-type units per 7×2 unit cell, whereby the two A-type units arrange in the staggered configuration of the $c(4\times2)$ surface. Regions with $c(4\times2)$ configuration have also been observed in experiment between Si ad-dimer lines.[29] Actually, for the 7×2 reconstruction, we find the nearest neighbor A-block lines on the left and right hand side of the B line to be shifted with respect to one another by half a surface lattice constant (i.e., by 3.07 Å) along the $\times2$ direction. This mismatch of about 3 Å of the A-type units on the left and right hand side of the D_B ad-dimer line has been observed, as well.[29]

Figure 4 shows the surface band structure of the optimized TAADM according to Fig. 2. Within the fundamental band gap, there are three occupied (D_{A1}, D_{A2}, D_B) and three empty ($D^\star_{A1}$, $D^\star_{A2}$, $D^\star_B$) surface state bands originating from

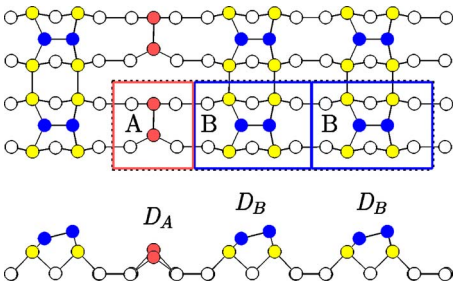

FIG. 5. (Color online) Top and side view of the optimal 8×2 TAAD model. For details, see caption of Fig. 1.

bonding and antibonding states of the localized dangling bonds at the two dimers D_A and the dimer D_B per unit cell, respectively. The 7×2 surface clearly turns out to be semiconducting. The occupied bands D_{A1} and D_{A2}, as well as the empty bands $D^{\star}_{A1}$ and $D^{\star}_{A2}$ show only small splittings due to the weak interaction between the D_A dimers of the two A-type blocks in each unit cell. To the best of our knowledge, no data on surface electronic properties of the 7×2 surface have been reported, to date.

C. The SiC(001)-(8×2) surface

We now address the 8×2 reconstruction. Again, we expect that most simple superpositions of A-type and B-type building blocks with a minimum of surface dangling bonds yield favorable locally stable total energy minimum configurations. Following this notion by a careful analysis of 8×2 reconstructions in the framework of DFT-LDA calculations, we have distributed Si adatoms in the 8×2 surface unit cell similar to those in one $c(4\times2)$ and two 3×2 unit cells to allow again for a minimization of the number of surface dangling bonds. Starting with a number of such different adatom distributions, we end up with the total energy minimum configuration shown in Fig. 5 by a top and a side view. Also for the 8×2 reconstruction, we find the TAAD model to be a locally stable energy minimum configuration. There are again two partial adlayers above the Si sublayer now with 1/4 and 5/8 of a Si monolayer from top to bottom. The atomic positions in the 8×2 unit cell again turn out to be very similar to those in one respective $c(4\times2)$ and two respective 3×2 unit cells. Thus, the 8×2 reconstruction turns out to consist of one A-type and two B-type building blocks per 8×2 unit cell and the number of surface dangling bonds is only six, as in the case of the 7×2 surface. In this particular case of the 8×2 surface, there are only two ways of arranging the single A-type block with respect to the two B-type blocks in the unit cell. One is shown in Fig. 5. The other results if we shift the A-type block by half a surface lattice constant along the $\times2$ direction. Since the Si atoms on the two top adlayers belonging to the different A-type and B-type building blocks do only interact marginally, this shift changes the total energy by less than 0.005 eV. The physical properties of both structures are practically the same, again. For simplicity, we address, in the following, the surface structure shown in Fig. 5 as the 8×2 reconstruction, therefore.

Also in the case of the 8×2 surface, the D_B dimers occur significantly higher above the surface than the D_A dimers (see bottom panel of Fig. 5). The height of the two D_B dimers per unit cell agrees within 0.001 Å and the upper one of them is 1.301 Å higher above the surface than the D_A dimer. Thus, in this case, the D_B dimers in the B-type building blocks give rise to pairs of Si ad-dimer lines in an 8×2 periodic arrangement along the $\times2$ direction interspaced by one channel of lower lying D_A dimers (see top panel of Fig. 5) which appear as missing dimer lines in STM. The D_B ad-dimers are oriented perpendicular to these lines while the D_A ad-dimers forming lines on the lower adlayer of the surface are oriented parallel to the lines. A respective periodic structure of ad-dimer line pairs has been observed at the 8×2 surface in STM images by Douillard *et al.*[30] The STM images very clearly show a periodic arrangement of pairs of ad-dimer lines with the dimers stacked perpendicular to the lines and a missing line in between. This result clearly rules out the generalized DDRM of Hara *et al.*[19] in which the ad-dimers are oriented parallel to the dimer lines (cf. Ref. 31). In addition, the latter model has fourteen dangling bonds per surface unit cell while our 8×2 TAADM has only six. Doulliard *et al.*[30] have suggested a model for the 8×2 surface consisting of a superposition of 3×2 and 5×2 units which they assumed to reconstruct[19,21,30] according to the SDRM. This latter model has been discarded in the meantime, however, on the basis of *ab initio* results,[34–36] as well as on the basis of new experimental results of Soukiassian's group.[47,50,51]

Thus, our 8×2 structure is an *ABB* reconstruction exhibiting one D_A and two D_B ad-dimers per surface unit cell. The distances between neighboring D_B lines in the surface unit cell, neighboring surface unit cells, and neighboring D_B dimers along the lines are simply determined by symmetry and are given by $d_1=3a_0=9.21$ Å, $d_2=8a_0=24.56$ Å, and $d_3=2a_0=6.14$ Å, respectively, where a_0 is the surface lattice constant which results from our calculations as $a_0=3.07$ Å. The above mentioned distances were found in STM to be $d_1=9\pm1$ Å, $d_2=25\pm1$ Å, and $d_3=5.8\pm0.9$ Å, respectively.[30] The close agreement between these theoretical and experimental values concerning the global structure of the surface is merely a consequence of the fact that both theory and experiment find an 8×2 reconstruction consisting of pairs of ad-dimer lines interspaced by one missing line. Our results allow us, in addition, to identify the internal microscopic structure within each 8×2 unit cell. The 8×2 TAADM consists of a superposition of one $c(4\times2)$ and two 3×2 blocks. Actually, it can be viewed as a superposition of one 3×2 and one 5×2 block since the 5×2 block contains one $c(4\times2)$ and one 3×2 block. So our 8×2 TAADM reveals the internal structure of the surface unit cell, consists of a superposition of 3×2 and 5×2 units, is a total energy minimum structure and allows us to explain the experimental findings.[30] In experiment it was observed that the two Si dimer lines belonging to the same pair have the same respective positions as the single dimer lines at the 3×2 surface.[30] Our *ABB* model of the 8×2 surface readily explains this finding since each B-type unit in the *ABB* structure has practically the same geometry as the B unit of the 3×2 surface.

In spite of the close agreement between theory and experiment on the topology of the 8×2 reconstruction, one

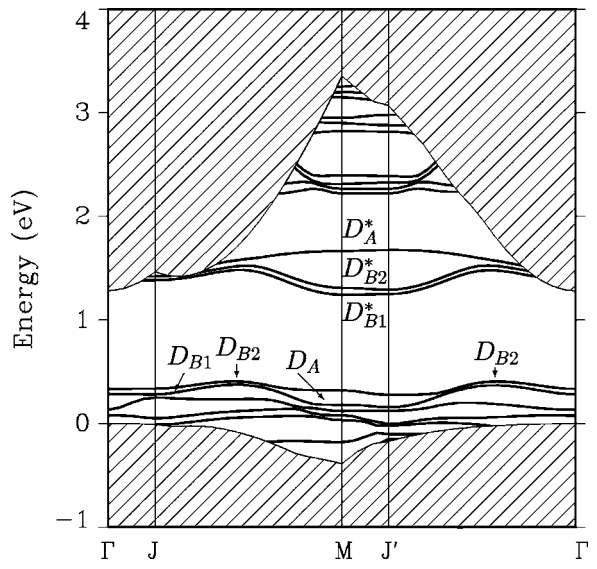

FIG. 6. Surface electronic structure of the TAADM of SiC(001)-(8×2) according to Fig. 5.

quantitative difference remains to be resolved. While we find the dimers to be asymmetric at the 3×2, 5×2, and 8×2 surfaces, they are found in experiment to be asymmetric at the 3×2 surface[21] but symmetric at the 8×2 surface.[30,31] A similar discrepancy between theory and experiment concerning the buckling of topologically equivalent Si dimers on the Si(001) surface has led to a long-standing discussion. In that case, the dimers appear symmetric in STM images taken at room temperature,[56] while they are found in low-temperature STM[57] to be asymmetric at $T<10$ K. To the best of our knowledge, the STM investigations of the SiC(001)-($n\times2$) surface[30,31] have been carried out at room temperature after annealing the samples at specific high temperatures. So far, no low-temperature STM images of the 8×2 surface seem to be available in the literature which might exhibit asymmetric dimers as resulting from our calculations.

Figure 6 shows the surface band structure of the 8×2 TAADM according to Fig. 5. Within the fundamental band gap, there are three salient occupied (D_A, D_{B1}, D_{B2}) and three empty ($D_A^\star$, $D_{B1}^\star$, $D_{B2}^\star$) surface state bands which originate from bonding and antibonding states of the localized dangling bonds at the two D_B dimers and the D_A dimer, respectively. Like the 7×2 surface, also the 8×2 surface is clearly semiconducting. The occupied bands D_{B1} and D_{B2}, as well as the empty bands $D_{B1}^\star$ and $D_{B2}^\star$ show small splittings due to the weak interaction between the D_B dimers on the two B-type building blocks. To the best of our knowledge, no data on the surface electronic structure of the 8×2 surface have been reported, to date. There are some interesting facts about the band structures of the 7×2 and 8×2 surfaces to be noted. We recall that at the 7×2 surface, there are two D_A dimers and one D_B dimer, while at the 8×2 surface there are two D_B dimers and one D_A dimer per unit cell. Comparing the surface band structures in Figs. 4 and 6, it becomes immediately obvious that the two D_B and the two $D_B^\star$ bands at the 8×2 surface are very close to the one D_B and the one $D_B^\star$ band at the 7×2 surface, respectively, and they are only slightly split due to the very weak interaction of the two D_B dimers at the 8×2 surface. Conversely, the two D_A and the two $D_A^\star$ bands at the 7×2 surface show the respective behavior when compared to the one D_A and the one $D_A^\star$ band at the 8×2 surface, respectively. Again the splittings of the former are very small and they are close to the respective D_A and $D_A^\star$ bands at the 8×2 surface, respectively.

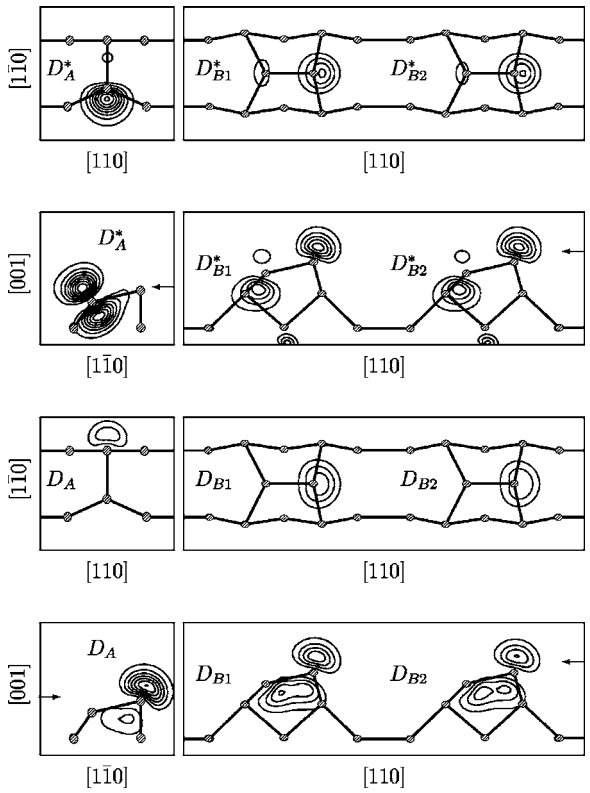

FIG. 7. Charge-density contours of the empty ($D_A^\star$, $D_{B1}^\star$, and $D_{B2}^\star$) and occupied (D_A, D_{B1}, and D_{B2}) dangling bond states at the M point of the SBZ. The two top and bottom panels show the empty and occupied states by top views (first and third panel) and side views (second and fourth), respectively. The plotting planes for the side views contain the respective dimers. The position of the plotting planes for the top views in the [001] direction are indicated by arrows in the corresponding side views.

Charge densities of the most salient surface states at the M point of the SBZ are shown in Fig. 7. Obviously, all these states are strongly localized at either the D_A dimer of the A-type or the D_B dimers of the two B-type building blocks (see also Fig. 5), respectively. We show in Fig. 7 sums of respective charge densities of all three dangling bond states for shortness's sake. Our detailed results on all separate charge densities clearly reveal that the dangling bond states of the D_A dimer do not couple at all to those at the D_B dimers, while the D_B dimers show a very weak coupling in the sense that, e.g., the charge density of the D_{B1} state of the left B-type block has a very small contribution also on the D_B dimer on the right B-type block. We have addressed this very small coupling already in context with the respectively small splitting of the surface state bands resulting from D_{B1} and D_{B2} states in Fig. 6. Obviously, the charge densities of the dangling bond states on the two B-type blocks, shown in

the right sections of the four panels in Fig. 7, show only very small differences. These are related to the fact that the Si down atom of the left D_B dimer has a D_A dimer as its neighbor on the left while the Si up atom of the right D_B dimer has a D_A dimer as its neighbor on the right. Most interestingly, the side views of the dangling bond states resulting from dimer D_A have the same character as those found at the SiC(001)-$c(4\times2)$ surface[25] or at the Si(001)-(2×1) surface.[59] The occupied dangling bond state D_A corresponds to D_{up} and the empty dangling bond state $D_A^\star$ corresponds to D_{down} since they are entirely localized at the dimer up or down atom, respectively. These dimers reside on a complete Si sublayer as is typical for the other cases mentioned above. On the contrary, the dimer dangling bond states related to the D_B dimers are now somewhat more intricate. The occupied states D_{B1} and D_{B2} remain localized at the dimer up atoms with a somewhat more extended charge density between the first and second layer within the dimers (compare left and right side in the bottom panel of Fig. 7) but they could still be labeled D_{up} states. The empty states, on the contrary, are now antibonding states resulting from wave function contributions at both the dimer up and down atoms and are very different from $D_A^\star$ (compare left and right side in the second panel of Fig. 7). This difference originates from the fact that the top adlayer D_B dimers reside on the lower Si adlayer which contains only 2/3 of a full Si monolayer. Some of these changes are due to substrate-mediated interactions and they do occur because of the spatially more open boundary conditions left and right from the *BB* sections in the *A* channels which have only one partial adlayer. In summary, both the surface electronic structure and the charge densities of the 8×2 surface clearly reveal that the surface electronic properties of the 8×2 reconstruction separate into those of one *A*-type and two *B*-type building blocks.

We have also analyzed the other bands of localized surface states in Fig. 6. For shortness's sake, we refrain from showing their charge densities and discussing their character in detail, as well. We just mention that they originate from bonding and antibonding states of back bonds between the second and third layer, as well as of dimer bonds on the third layer. Their wave function character is sensitively dependent on the surface-parallel wave vector. Even surface-induced changes of the carbon states on the fourth layer give rise to a band of surface states in a restricted section of the SBZ.

IV. GENERALIZED TAAD MODEL

In this section, we first describe our general model for $n\times2$ reconstructions which we infer from a generalization of the *ab initio* results for the 5×2, 7×2, and 8×2 reconstructions discussed in Sec. III. We then show that this general model can be very accurately described within an excellent approximation by simply employing exactly the same building blocks *A* and *B*, as resulting from our *ab initio* calculations for the $c(4\times2)$ and 3×2 surface.

A. General model

From the preceding discussion, it is now quite obvious how to extend the TAAD model to higher $n\times2$ reconstructions. We have shown in Sec. III that the atomic structure of the 5×2, 7×2, and 8×2 reconstructions of SiC(001) result as simple *AB*, *AAB*, and *ABB* superpositions of entire *A*-type and *B*-type building blocks from our first-principles calculations. On the basis of these results, we feel confident to extrapolate our TAADM to higher n values and suggest higher $n\times2$ reconstructions as appropriate superpositions of *A*-type and *B*-type building blocks in the $n\times$ direction corresponding to the above examples. This way, the Si sublayer dangling bonds are fully saturated, in each case, reducing the number of surface dangling bonds of each particular reconstruction to a minimum. The unit cells of respective $n\times2$ reconstructions that can be formed this way consist of l *A*-type and m *B*-type building blocks.[52] We label them A_lB_m reconstructions, correspondingly. Since the *A*-type and *B*-type blocks have exactly the lengths 2 and 3 in the $n\times$ direction (in units of the surface lattice constant), respectively, the possible $n>3$ values are given by

$$n = 2l + 3m \tag{2}$$

with $l\geqslant1$ and $m\geqslant1$. The case $l=1$, $m=0$ would be the 2×2 MRAD model which is less favorable than the $c(4\times2)$ reconstruction, as discussed, and which constitutes a one adlayer asymmetric dimer row model, in particular. To specify the general $n\times2$ TAADM uniquely, we note that for $l>1$ the *A*-type blocks arrange in the staggered $c(4\times2)$ pattern to yield the energy minimum configuration, as we have discussed, e.g., for the 7×2 *AAB* reconstruction in Sec. III. For $l=1$, there is only one *A* block per unit cell (see, e.g., bottom panel of Fig. 1 or top panel of Fig. 5) so that there is no need for a respective specification.

The Si coverage of a $n\times2$ surface including the complete Si sublayer is given within the general TAADM as

$$\Theta_{n\times2} = 1 + (l + 3m)/(2l + 3m) \tag{3}$$

with n as defined in Eq. (2). For large m, the coverage $\Theta_{n\times2}$ approaches 2 and for small m it approaches 1.5, the coverages of the 3×2 TAADM and the $c(4\times2)$ MRAD model, respectively. The Si coverage of our general TAADM thus decreases from that of the silicon-rich 3×2 to that of the silicon-poor $c(4\times2)$ surface (cf. Refs. 5, 18, and 33) in the order of $\Theta_{3\times2}>\Theta_{5\times2}>\Theta_{7\times2}>\Theta_{c(4\times2)}$ as $2.0>1.8>1.71>1.5$ consistent with medium-energy ion scattering data.[18] In addition, the Si dose required to prepare the silicon-rich 3×2 and 5×2 surfaces was found in experiment to be approximately 1.36 and 1.16 times as large as the dose necessary for preparing the $c(4\times2)$or 2×1 surfaces.[58] From our TAADM $\Theta_{3\times2}/\Theta_{c(4\times2)}$ and $\Theta_{5\times2}/\Theta_{c(4\times2)}$ result as 1.33 and 1.2 in gratifying agreement with experiment.

The n values possible within our model follow directly from Eq. (2). They reveal a number of interesting features: (1) Neither a primitive 4×2 nor a 6×2 reconstruction occurs in agreement with experiment. Such reconstructions have never been reported, to date. (2) Higher $n\times2$ reconstructions for all $n\geqslant7$ can occur. The first even reconstruction is the 8×2 as observed in experiment.[30,31] Interestingly, those with n values of 3, 5, and 7 to 10 have one realization, only, while there are two or more realizations for all other

reconstructions. The 11×2 surface, e.g., can be an A_4B_1 or an A_1B_3, the 15×2 surface can be an A_6B_1 or an A_3B_3, and the 17×2 surface can be an A_7B_1, an A_4B_3, or an A_1B_5 reconstruction. (3) The 8×2 surface constitutes an AB_2 reconstruction, as discussed in detail in Sec. III, explaining the respective experimental observations. (4) All $n\times2$ reconstructions have periodic arrays of one or more Si ad-dimer lines of B-type units along the $\times2$ direction which are spatially separated by lines of A-type units for $n\geqslant 5$. Since the D_B dimers reside significantly higher above the surface than the D_A dimers (see, e.g., the side views in Figs. 2 and 5) the former are preferentially observable in filled-state STM images where they appear as Si ad-dimer lines along the $\times2$ direction, as observed by Kitamura *et al.*[33] In their STM images, periodic arrays of Si nanolines in 3×2, 5×2, 8×2, and 15×2 configurations are clearly visible.[33] The latter STM image, in particular, shows the A_3B_3 realization of the 15×2 reconstruction while the mixed 3×2 and 5×2 structures show ad-dimer strings characteristic for the 5×2 or 8×2 reconstructions. (5) All A_lB_1 reconstructions have only one D_B ad-dimer line along the $\times2$ direction per unit cell. These are separated by l lines of A-type blocks appearing as missing rows between the D_B lines. For large l values, the ad-dimer lines appear in these cases as single lines although they occur periodically at the surface.

Within the above presented general model the possible A_lB_m configurations of $n\times2$ reconstructions are well defined in terms of the basic A-type and B-type building blocks characteristic for the $c(4\times2)$ and 3×2 surfaces, respectively.[52] Yet, the exact atomic positions in a given higher $n\times2$ reconstruction would have to be calculated fully quantitatively by additional *ab initio* total energy minimization for each considered reconstruction allowing all atoms in the $n\times2$ unit cell to relax to their optimal positions. This is extremely demanding for large n values. On the basis of our results it appears, as a matter of fact, that such calculations are not really necessary, as we will show in Sec. IV B.

B. Simplified description of the general model

Instead of the general A-type and B-type building blocks deviating slightly from those of the $c(4\times2)$ and 3×2 surfaces, we now employ in the TAADM *exactly* the A and B building blocks of the latter two surfaces. The structure of all resulting $n\times2$ surfaces is then simply known without the need of any further calculations. Using the atomic positions of the A and B blocks given in the appendix the structure of higher $n\times2$ reconstructions can readily be calculated. For a given $n\times2$ reconstruction, we do not expect it to show any significant deviation from the results of a full first-principles total-energy minimization calculation in view of our respective results for the 5×2, 7×2, and 8×2 reconstructions which show deviations in atomic distances within 1% only.

In addition, it is very revealing that the formation energies of the 5×2, 7×2, and 8×2 surfaces as simply obtained from corresponding sums of the formation energies of A and B units are very close to the values resulting from our first-principles calculations. The formation energies per $n\times2$ unit cell are given within this simplified description of the TAADM by

TABLE I. Comparison of surface formation energies per unit cell (in eV) for $\mu_{Si}=\mu_{Si(bulk)}$, as resulting from our LDA calculations and from the simplified description of the TAADM according to Eq. (4). Formation energies per 1×1 unit cell are given in the last two columns, for convenience.

$n\times2$	A_lB_m	$E_{f,n\times2}^{LDA}$	$E_{f,n\times2}^{TAADM}$	$E_{f,n\times2}^{LDA}$	$E_{f,n\times2}^{TAADM}$
$c(4\times2)$	A_1	−2.568		−0.642	
3×2	B_1	−5.692		−0.949	
5×2	A_1B_1	−8.291	−8.260	−0.829	−0.826
7×2	A_2B_1	−10.868	−10.827	−0.776	−0.773
8×2	A_1B_2	−13.992	−13.952	−0.875	−0.872
9×2	A_3B_1		−13.395		−0.744
10×2	A_2B_2		−16.520		−0.826

$$E_{f,n\times2}^{TAADM}=lE_{f,c(4\times2)}^{LDA}+mE_{f,3\times2}^{LDA} \tag{4}$$

with the two DFT-LDA values for the $c(4\times2)$ and 3×2 surfaces (per respective unit cell) entering Eq. (4) given in Table I. The table very clearly exhibits how closely the results of this simplified description of the TAADM agree with our *ab initio* LDA results for the 5×2, 7×2, and 8×2 surfaces. The formation energies differ in all cases by less than 0.4% agreeing within 3 meV per 1×1 unit cell. These results again corroborate that the substrate sections of the A-type and B-type building blocks of the 5×2, 7×2, and 8×2 surfaces are very similar to those of the $c(4\times2)$ and 3×2 surfaces, respectively, and that there is only marginal interaction between the Si adatoms belonging to the different A-type and B-type building blocks. For the D_A and D_B dimers in the different surface unit cells this is most obvious since they have a large lateral (7.7 Å) and vertical (1.3 Å) separation and they are oriented orthogonal to each other, in particular (see, e.g., top panels of Figs. 2 and 5).

The very close agreement between the surface structures and formation energies of the general TAADM for the 5×2, 7×2, and 8×2 surfaces with the respective results following from its simplified description shows the appropriateness and accuracy of the latter. We expect this to obtain for higher $n\times2$ reconstructions, as well. The simplified description thus turns out to be an extremely useful approximation of the general TAADM and to be largely equivalent to it for all practical purposes. The above agreement should be valued in view of the fact that both the atomic coordinates and the formation energies of $n\times2$ reconstructions can be calculated "on the back of an envelope" using the structure data in the Appendix and Eq. (4), while the respective *ab initio* results for higher $n\times2$ reconstructions require very demanding new self-consistent calculations in each case. In each case, the structure of a $n\times2$ reconstruction obtained in this simple way can serve as an excellent starting configuration for a full *ab initio* calculation if it is deemed necessary. Moreover, on the basis of our experience with the 5×2, 7×2, and 8×2 surfaces, we expect that the surface electronic structure of higher $n\times2$ reconstructions can readily be calculated when surface spectroscopy data become available using the atomic structure resulting from the simplified de-

scription of the general TAADM without loss of any significant accuracy.

We note in passing that the simplified description can easily be made even more accurate by a single extension employing the *ab initio* results for the 5×2 reconstruction on input, as well. This is due to the fact that any A_lB_m reconstruction features in general neighboring A, B, and AB units. So far, we have approximated the AB unit as a superposition of one A and one B block but this description does not grasp the properties of the 5×2 AB reconstruction fully quantitatively, as mentioned above.[52] If we want to account completely for the latter, we only need to employ the *ab initio* results for the 5×2 AB reconstruction, in addition. This way, we include the interactions between different A, B, and AB blocks very accurately. The formation energies of $n\times2$ reconstructions with $n\geqslant 7$ are then simply given by respective sums of the formation energies of A, B, and AB units. Using for the A, B, and AB units the appropriate LDA formation energies of the $c(4\times2)$, 3×2, and 5×2 reconstructions from Table I, we obtain for the 7×2 $A_1(AB)_1$ and the 8×2 $(AB)_1B_1$ reconstructions formation energies per unit cell of -10.859 eV and -13.983 eV, to be compared to the LDA results of -10.868 eV and -13.992 eV, respectively (see Table I). These values now differ by less than 0.08% agreeing within 9 meV per $n\times2$ and within better than 1 meV per 1×1 unit cell. This close agreement strongly emphasizes that the physical properties of higher $n\times2$ reconstructions can practically be described quantitatively employing the *ab initio* results on the $c(4\times2)$, 3×2, and 5×2 surfaces on input. This way, we obtain for the 9×2 $A_2(AB)_1$ and 10×2 $A_1(AB)_1B_1$ reconstructions formation energies of -13.427 eV and -16.551 eV. They are also some 30 meV lower than the respective values in Table I. These improvements, however, have no significant bearing on the physical properties of Si ad-dimer strings to be addressed in Sec. V, while they slightly increase the complexity of the simplified description of the TAADM. Therefore, we stick to employing exactly the A and B building blocks of the $c(4\times2)$ and 3×2 surfaces.

V. SI AD-DIMER STRINGS

Finally, we address the experimentally observed formation of Si lines or nanostrings self-organizing or self-assembling on SiC(001) surfaces. If they occur in regular arrays on periodic $n\times2$ surfaces, as discussed above, the Si ad-dimer lines are just part of the periodic surface structure. If they self-assemble in irregular nonperiodic arrangements on a large surface area, they are one-dimensional subnanometer Si structures or ad-dimer strings. A large variety of nanostring configurations has been observed depending crucially on surface preparation conditions (cf. Ref. 8). Si nanostrings are always found to be oriented parallel to one another in the $\times2$ direction even if they are very far apart from each other but they do not necessarily form periodic arrangements in the perpendicular $n\times$ direction.[7,8,29–33,60] These findings can be rationalized within our TAAD model. To address the experimental observations, we have calculated formation energies of the $c(4\times2)$ and a number of $n\times2$ reconstructions according to Eq. (4). For a meaningful comparison, they are normalized to a 1×1 unit cell, i.e., they are divided by $2n$. Referring all these formation energies to that of the 3×2 surface, we obtain *relative* formation energies which are shown in Fig. 8 for the $c(4\times2)$ and a number of $n\times2$ reconstructions up to $n=11$, only, for clarity's sake. First, we note that for silicon-poor and silicon-rich conditions, the $c(4\times2)$ MRAD and the 3×2 TAAD reconstructions are lowest in formation energy, respectively. This is in agreement with all experimental evidence on Si-terminated SiC(001) surfaces (cf. Refs. 5, 7, 8, 18, 19, 29–33, 50, and 51). Next, we observe that the formation energies of all other $n\times2$ reconstructions in Fig. 8 fall between these two limiting cases. Actually, the line for the 5×2 reconstruction separates the relative formation energies for all A_lB_1 and A_1B_m reconstructions. The former occur between the 5×2 and $c(4\times2)$ graphs while the latter result between the 5×2 and 3×2 graphs. Note that the $A_\infty B_1$ reconstruction is practically the $c(4\times2)$ A_1 reconstruction while the A_1B_∞ reconstruction is practically the 3×2 B_1 reconstruction. Obviously, a 10×2 A_2B_2 reconstruction is structurally inequivalent to a 5×2 A_1B_1 reconstruction. But within the simplified description of the TAADM, they have both identical formation energies per 1×1 unit cell (see Table I). The same holds for the 15×2 A_3B_3 and the 20×2 A_4B_4 reconstructions. The energetic equivalence of these latter A_mB_m reconstructions strictly follows from the simplified description, but we expect it to hold largely for the general TAADM, as well, due to the marginal residual interactions between Si adlayer atoms belonging to the different A-type and B-type building blocks. Most interestingly, all graphs in Fig. 8 intersect at the value μ_{Si}^{crit} for which the formation energies of the A and B building blocks become equal. This basic result from the simplified description is corroborated by our *ab initio* calculations for the 5×2, 7×2, and 8×2 surfaces within less than 3 meV. From

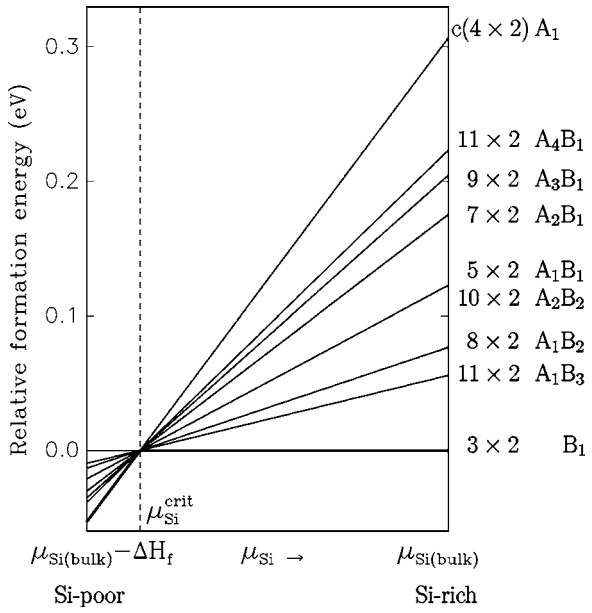

FIG. 8. Relative formation energies (referred to E_f of the 3×2 reconstruction and normalized to the 1×1 unit cell) of the $c(4\times2)$ and $n\times2$ surfaces (lowest possible n only) of SiC(001) as a function of μ_{Si}.

the intersection in Fig. 8, the critical value results as $\mu_{Si}^{crit} = \mu_{Si(bulk)} - 0.61$ eV. In experiment, higher $n\times2$ reconstructions are found "between" the $c(4\times2)$ and the 3×2 reconstructions (cf. Refs. 5 and 8). For example, Douillard *et al.*[30] observe the 8×2 reconstruction which they consider as a novel intermediate structure at the transition between the 3×2 and 5×2 reconstructions. The placement of the relative formation energy of the 8×2 reconstruction between those of the 3×2 and 5×2 surfaces in Fig. 8 can be viewed as an indication for this experimental finding, in particular when μ_{Si} is close to μ_{Si}^{crit}. Furthermore, Kitamura *et al.*[33] observe 5×2, 8×2, and 15×2 reconstructions at the same sample surface during the phase transition between the $c(4\times2)$ and 3×2 surface.

The above statements apply for all higher periodic $n\times2$ reconstructions and, most importantly, for all nonperiodic arrangements of lines of *A* and *B* building blocks along the $n\times$ direction, as well. Thus many different configurations of D_B ad-dimer lines along the $\times2$ direction interspaced by respective numbers of D_A dimer lines appearing as missing dimer lines in STM can occur either as periodic $n\times2$ reconstructions or as nonperiodic Si nanostring arrangements along the $n\times$ direction. When the preparation conditions are chosen such that μ_{Si} is near μ_{Si}^{crit}, in particular, all of such different Si ad-dimer string configurations (D_B lines) can coexist at the SiC(001) surface resulting in arrangements ranging from a very large $n\times2$ superlattice to a single isolated atomic line, as observed in experiment (cf. Refs. 29–33 and 60). The subsurface on which these lines are lying (the *A* block areas) then shows the $c(4\times2)$ reconstruction as observed in experiment as well.[29,31,32] It was also seen that the Si atomic lines follow the underlying surface registry. This means that they are parallel to the lines of *A* building blocks in the $\times2$ direction resulting from our model. Likewise, it becomes obvious that for appropriately chosen experimental conditions (annealing time and temperature or Si gas pressure), i.e., for an appropriately chosen μ_{Si}, different $n\times2$ arrangements with $n\geqslant5$ can occur although the 3×2 and $c(4\times2)$ surfaces are the formation energy minimum structures for silicon-rich or silicon-poor conditions at $T=0$ K, respectively. The chemical potential becomes smaller with increasing temperature corresponding to increasingly silicon-poor conditions. Therefore, by annealing a Si-saturated surface, one moves to the left hand side in the plot of Fig. 8 where the lines for all structures are very close in formation energy. A large thermal energy will then allow one to experimentally realize structures other than the 3×2 or $c(4\times2)$ reconstructions, respectively, albeit that the curves in Fig. 8 certainly change for higher temperatures to a certain extent. Annealing a 3×2 surface for a short time at 1150 °C, for example, Douillard *et al.*[30] find neighboring regions of straight parallel ad-dimer lines arranged in more or less dense patterns. The dense line arrangements correspond to remaining 3×2 reconstruction areas, while the less dense regions correspond to 5×2 or 8×2 reconstruction areas with one or two neighboring lines and one missing line in between (see, e.g., the side view of Fig. 5). For μ_{Si} near μ_{Si}^{crit}, all of such areas are very close in formation energy (per 1×1 unit cell) so that they can easily coexist. This situation is reminiscent of the polytypism of bulk SiC, which is closely related to the very small energy differences between different stackings of Si-C double layers and the respective differences in the interaction energy between neighboring double layers (cf. Refs. 3 and 4). The same general notion applies near the critical value of the Si chemical potential to the arrangement of *A*-type and *B*-type dimer lines along the $\times n$ direction giving rise to many possible $n\times2$ reconstructions which are energetically very close.

For a quantitative theory of the self-assembly of Si ad-dimer nanolines at $T>0$ K under experimental conditions, one would have to take the configurational entropy of the system into account. This is beyond the scope of our current calculations. Our aim, instead, was to rationalize that periodic and nonperiodic arrangements of parallel Si ad-dimer nanolines can occur at the 3C-SiC(001) surface with all dimers stacked perpendicular to the line direction, as experimentally observed. In theory, these nanolines are infinitely long due to the usual periodic boundary conditions parallel to the surface. In experiment, they are found as nanostrings with finite lengths up to 1 μm terminated by ad-dimer defects in the lines or by surface steps.

VI. SUMMARY

We have presented the first *ab initio* investigation of structural and electronic properties of the 7×2 and 8×2 reconstructions of cubic SiC(001) surfaces and have discussed the outcome of our calculations in light of our previous results on the $c(4\times2)$, 3×2, and 5×2 reconstructions. The surface structural properties are found in gratifying agreement with most of the experimental data allowing for a detailed microscopic interpretation of the latter. The surface electronic properties have briefly been presented but could not yet be compared with experiment due to the lack of respective surface spectroscopy data. We have found that the 5×2, 7×2, and 8×2 reconstructions can be described in terms of two structural building blocks, only, which are characteristic for the $c(4\times2)$ and 3×2 surfaces. This observation allowed us to suggest a general two adlayer asymmetric dimer model for a host of $n\times2$ reconstructions, which explains a wealth of experimental observations on $n\times2$ surfaces and allows us to identify the origin and physical character of many different locally stable $n\times2$ reconstructions. In particular, we have shown that this model can easily be simplified within an excellent approximation by just employing exactly the two building blocks *A* and *B* of the $c(4\times2)$ and 3×2 surfaces, respectively. Once this marginal approximation is made, the atomic structure and formation energy of higher $n\times2$ reconstructions are known and their electronic structure can readily be calculated if necessary. Most importantly, our TAADM allows us to rationalize the occurrence of a wealth of Si ad-dimer-string configurations at the Si-terminated SiC(001) surface, as observed in experiment.

ACKNOWLEDGMENT

We acknowledge the support of this work by a grant of computer time on the JUMP computer of the John von Neu-

TABLE II. Coordinates of the atoms in the Si adlayer (ad) and the three topmost SiC layers (1st, 2nd, and 3rd) for the MRAD model of SiC(001)-$c(4\times2)$. All coordinates are given in Å. The x and y directions correspond to the $n\times$ and $\times2$ directions in Fig. 1. The z direction is perpendicular to the surface (i.e., parallel to the [001] direction) pointing out of the drawing plane in Fig. 1. The lower left corner of the quadratic cross section of building block A (red square in top panel of Fig. 1) is at the origin of the x and y coordinates.

Layer	Atom	x	y	z
ad	Si	3.069	4.569	4.958
	Si	3.069	2.347	4.414
1st	Si	1.192	1.538	3.244
	Si	1.348	4.591	3.262
	Si	4.946	1.538	3.244
	Si	4.789	4.591	3.262
2nd	C	1.510	−0.003	2.195
	C	1.495	3.069	2.145
	C	4.627	−0.003	2.195
	C	4.643	3.069	2.145
3rd	Si	0.011	−0.002	1.047
	Si	−0.011	3.066	1.047
	Si	3.069	0.008	1.122
	Si	3.069	3.064	1.097

man Institute for Computing (NIC) of the Forschungszentrum Jülich (Germany) under Contracts No. HMS08/1678 and HMS08/1897.

APPENDIX

In this appendix, we give the coordinates of the atoms in the A and B building blocks of the $c(4\times2)$ and 3×2 surfaces on the Si adlayers and the first three SiC substrate layers (Tables II and III, respectively) as resulting from our total-energy minimization calculations. The atoms on the three lower substrate layers used in the calculations are fixed at their bulk positions for the theoretical lattice constant of 4.34 Å. Using the coordinates of these blocks in the appropriate superposition for a particular $n\times2$ surface directly yields the structure of the possible A_lB_m reconstructions. The displacements of the atoms in the A and B blocks from their ideal positions and the tilts Δz of the asymmetric dimers can simply be determined from Tables II and III. We find, for example, for the D_A dimer at the $c(4\times2)$ surface $\Delta z_{c(4\times2)}=0.544$ Å and for the D_B dimer at the 3×2 surface $\Delta z_{3\times2}=0.530$ Å.

TABLE III. Coordinates of the atoms in the top and bottom Si adlayers (adt and adb) and the three topmost SiC layers (1st, 2nd, and 3rd) for the TAAD model of SiC(001)-(3×2). The lower left corner of the rectangular cross section of building block B (blue rectangle in the middle panel of Fig. 1) is at the origin of the x and y coordinates. For further details, see caption of Table II.

Layer	Atom	x	y	z
adt	Si	3.776	3.069	5.751
	Si	5.960	3.069	6.281
adb	Si	2.820	1.196	4.815
	Si	2.820	4.941	4.815
	Si	6.348	1.218	4.834
	Si	6.348	4.920	4.834
1st	Si	1.192	1.525	3.204
	Si	1.192	4.613	3.204
	Si	4.617	1.477	3.273
	Si	4.617	4.660	3.273
	Si	7.983	1.523	3.220
	Si	7.983	4.615	3.220
2nd	C	1.494	0.000	2.140
	C	1.508	3.069	2.177
	C	4.590	0.000	2.128
	C	4.611	3.069	2.249
	C	7.700	0.000	2.142
	C	7.699	3.069	2.177
3rd	Si	−0.009	0.000	1.035
	Si	−0.004	3.069	1.051
	Si	3.049	0.000	1.083
	Si	3.064	3.069	1.118
	Si	6.145	0.000	1.084
	Si	6.146	3.069	1.116

[1] *Silicon Carbide, Fundamental Questions and Applications to Current Device Technology*, edited by W. J. Choyke, H. Matsunami, and G. Pensl (Springer, Berlin, 2004).
[2] For further recent reviews, see J. Phys.: Condens. Matter **16**, S1555 (2004).
[3] W. R. L. Lambrecht, S. Limpijumnong, S. N. Rashkeev, and B. Segall, Phys. Status Solidi B **202**, 5 (1997).
[4] F. Bechstedt, P. Käckell, A. Zywietz, K. Karch, B. Adolph, K. Tenelsen, and J. Furthmüller, Phys. Status Solidi B **202**, 35 (1997).
[5] V. M. Bermudez, Phys. Status Solidi B **202**, 447 (1997).
[6] J. Pollmann, P. Krüger, and M. Sabisch, Phys. Status Solidi B **202**, 421 (1997).
[7] P. Soukiassian, Mater. Sci. Eng., B **B96**, 115 (2002).
[8] P. Soukiassian and H. B. Enriquez, J. Phys.: Condens. Matter **16**, S1611 (2004).

[9] J. Pollmann and P. Krüger, J. Phys.: Condens. Matter **16**, S1659 (2004).
[10] J. M. Powers, A. Wander, P. J. Rous, M. A. Van Hove, and G. A. Somorjai, Phys. Rev. B **44**, 11159 (1991).
[11] J. P. Long, V. M. Bermudez, and D. E. Ramaker, Phys. Rev. Lett. **76**, 991 (1996).
[12] P. Soukiassian, F. Semond, L. Douillard, A. Mayne, G. Dujardin, L. Pizzagalli, and C. Joachim, Phys. Rev. Lett. **78**, 907 (1997).
[13] H. W. Yeom, M. Shimomura, J. Kitamura, S. Hara, K. Tono, I. Matsuda, B. S. Mun, W. A. R. Huff, S. Kono, T. Ohta, S. Yoshida, H. Okushi, K. Kajimura, and C. S. Fadley, Phys. Rev. Lett. **83**, 1640 (1999).
[14] V. Derycke, P. Soukiassian, A. Mayne, and G. Dujardin, Surf. Sci. **446**, L101 (2000).
[15] A. Catellani, G. Galli, and P. L. Rigolli, Phys. Rev. B **62**, R4794 (2000).
[16] Fu-He Wang, P. Krüger, and J. Pollmann, Phys. Rev. B **66**, 195335 (2002).
[17] A. Catellani and G. Galli, Prog. Surf. Sci. **69**, 101 (2002).
[18] S. Hara, W. F. J. Slijkerman, J. F. van der Veen, I. Ohdomari, S. Misawa, E. Sakuma, and S. Yoshida, Surf. Sci. Lett. **231**, L196 (1990).
[19] S. Hara, S. Misawa, S. Yoshida, and Y. Aoyagi, Phys. Rev. B **50**, 4548 (1994).
[20] P. Soukiassian and F. Semond, J. Phys. IV **7**, C6–101 (1997).
[21] F. Semond, P. Soukiassian, A. Mayne, G. Dujardin, L. Douillard, and C. Jaussaud, Phys. Rev. Lett. **77**, 2013 (1996).
[22] M. L. Shek, Surf. Sci. **349**, 317 (1996).
[23] L. Douillard, F. Semond, V. Yu. Aristov, P. Soukiassian, B. Delley, A. Mayne, G. Dujardin, and E. Wimmer, Mater. Sci. Forum **264-268**, 379 (1998).
[24] L. Pizzagalli, C. Joachim, A. Mayne, G. Dujardin, F. Semond, L. Douillard, and P. Soukiassian, Thin Solid Films **318**, 136 (1998).
[25] W. Lu, P. Krüger, and J. Pollmann, Phys. Rev. Lett. **81**, 2292 (1998).
[26] W. Lu, P. Krüger, and J. Pollmann, Phys. Rev. Lett. **82**, 3722 (1998).
[27] J. M. Powers, A. Wander, M. A. Van Hove, and G. A. Somorjai, Surf. Sci. Lett. **260**, L7 (1992).
[28] H. Hüsken, B. Schröter, and W. Richer, Surf. Sci. **407**, 114 (1998).
[29] P. Soukiassian, F. Semond, A. Mayne, and G. Dujardin, Phys. Rev. Lett. **79**, 2498 (1997).
[30] L. Douillard, V. Yu. Aristov, F. Semond, and P. Soukiassian, Surf. Sci. **401**, L395 (1998).
[31] V. Derycke, N. P. Pham, P. Fonteneau, P. Soukiassian, P. Aboulet-Nze, Y. Monteil, A. J. Mayne, G. Dujardin, and J. Gautier, Appl. Surf. Sci. **162-163**, 413 (2000).
[32] V. Yu. Aristov, L. Douillard, and P. Soukiassian, Surf. Sci. **440**, L825 (1999).
[33] J. Kitamura, S. Hara, H. Okushi, Y. Yoshida, S. Misawa, and K. Kajimura, Surf. Sci. **433-435**, 465 (1999).
[34] W. Lu, P. Krüger, and J. Pollmann, Phys. Rev. B **60**, 2495 (1999).
[35] W. Lu, P. Krüger, and J. Pollmann, Phys. Rev. B **61**, 2680 (2000).
[36] S. A. Shevlin, A. J. Fisher, and E. Hernandez, Phys. Rev. B **63**, 195306 (2001).
[37] W. Kohn and L. J. Sham, Phys. Rev. **140**, A1133 (1965).
[38] L. Kleinman and D. M. Bylander, Phys. Rev. Lett. **48**, 1425 (1982).
[39] D. M. Ceperley and B. J. Alder, Phys. Rev. Lett. **45**, 566 (1980).
[40] J. P. Perdew and A. Zunger, Phys. Rev. B **23**, 5048 (1981).
[41] M. Sabisch, P. Krüger, A. Mazur, M. Rohlfing, and J. Pollmann, Phys. Rev. B **53**, 13121 (1996).
[42] H. J. Monkhorst and J. D. Pack, Phys. Rev. B **13**, 5188 (1976).
[43] G. Broyden, Math. Comput. **19**, 577 (1965).
[44] D. D. Johnson, Phys. Rev. B **38**, 12807 (1988).
[45] G-X. Qian, R. M. Martin, and D. J. Chadi, Phys. Rev. B **38**, 7649 (1988).
[46] J. E. Northrup and S. Froyen, Phys. Rev. Lett. **71**, 2276 (1993).
[47] Our $c(4\times2)$ MRAD and 3×2 TAAD models have been confirmed by *ab initio* calculations of Shevlin *et al.* (Refs. 36 and 48). The 3×2 TAADM has further been supported after its suggestion (Ref. 34) by reflectance anisotropy spectra (Ref. 49), grazing-incidence x-ray diffraction data (Ref. 50) and angle-resolved photoelectron spectroscopy data (Ref. 51). While for the 3×2 reconstruction general agreement on the TAADM has been achieved in recent years, the $c(4\times2)$ reconstruction remains to be a matter of controversial debate between theory and experiment. We note in passing that the alternatively up and down dimer (AUDD) model suggested earlier by Soukiassian *et al.* (Ref. 12) has four while our MRAD model has only two dangling bonds per surface unit cell. The MRAD model is thus significantly lower in total energy.
[48] S. A. Shevlin and A. J. Fisher, Phys. Rev. B **62**, 6904 (2000).
[49] W. Lu, W. G. Schmidt, E. L. Briggs, and J. Bernholc, Phys. Rev. Lett. **85**, 4381 (2000).
[50] M. D'angelo, H. Enriquez, V. Yu. Aristov, P. Soukiassian, G. Renaud, A. Barbier, M. Noblet, S. Chiang, and F. Semond, Phys. Rev. B **68**, 165321 (2003).
[51] A. Tejeda, D. Dunham, F. J. Garcia de Abajo, J. D. Denlinger, E. Rotenberg, E. G. Michel, and P. Soukiassian, Phys. Rev. B **70**, 045317 (2004).
[52] We refer to the building blocks as *A*-type and *B*-type whenever we want to stress that the precise atomic positions in these blocks, as resulting from total energy minimization for a given reconstruction with $n\geqslant5$, are slightly different from those of the *A* and *B* blocks of the $c(4\times2)$ and 3×2 surfaces, respectively, although the general structure of the blocks is the same.
[53] H. Yan, A. P. Smith, and H. Jónsson, Surf. Sci. **330**, 265 (1995).
[54] S. Hara, J. Kitamura, H. Okushi, S. Misawa, Y. Yoshida, and Y. Tokumaru, Surf. Sci. **357-358**, 436 (1996).
[55] J. Pollmann, P. Krüger, and W. Lu, Mater. Sci. Forum **338-342**, 369 (2000).
[56] R. M. Tromp, R. J. Hamers, and J. E. Demuth, Phys. Rev. Lett. **55**, 1303 (1985).
[57] M. Ono, A. Kamoshida, N. Matsuura, E. Ishikawa, T. Eguchi, and Y. Hasegawa, Phys. Rev. B **67**, 201306(R) (2003).
[58] T. Yoshinobu, I. Izumikawa, H. Mitsui, T. Fuyuki, and H. Matsunami, Appl. Phys. Lett. **59**, 2844 (1991).
[59] P. Krüger and J. Pollmann, Phys. Rev. Lett. **74**, 1155 (1995).
[60] H. W. Yeom, J. Electron Spectrosc. Relat. Phenom. **114**, 283 (2001).